Vega, M.; Venegas, M.; García-Hernando, N.; Ruiz-Rivas, U. (2015). Performance evaluation of H2O-LiBr absorber operating with microporous membrane technology. En: *First Thermal and Fluids Engineering Summer Conference* (9-12 August, 2015). New York: American Society of Thermal and Fluids Engineers (ASTFE).
DOI: 10.1615/TFESC1.mnt.012726

PERFORMANCE EVALUATION OF H_2O-LiBr ABSORBER OPERATING WITH MICROPOROUS MEMBRANE TECHNOLOGY

M. de Vega*, M. Venegas, N. García-Hernando, U. Ruiz-Rivas

[1]Universidad Carlos III de Madrid (UC3M), Avda. Universidad 30, 28911 Leganés, Madrid, Spain

ABSTRACT

With the aim of reducing the size and increasing the energy efficiency of absorption chillers, the use of microporous membrane technology in these systems is at present under study. In particular, the simulation of a H_2O-BrLi absorber using porous fibers for the heat and mass transfer between the solution and the vapor phase is considered in the present work. Heat and mass transfer process are modeled by means of selected correlations and data gathered from the open literature. Using the model developed, a simulation of the absorber is performed using typical operating conditions of absorption cooling chillers.

KEY WORDS: absorption refrigeration, membranes, heat and mass transfer, miniaturization, modeling, absorber

1. INTRODUCTION

Absorption chillers and heat pumps have received growing attention over the last few decades as they allow the use of low-grade heat to produce a cooling effect, with no (or minimal) mechanical power consumption. For example, absorption cooling machines can use waste heat or excess heat from solar collectors in the form of hot water for cooling purposes. In buildings, this could help to optimize the solar thermal energy in the summer period reducing the electricity consumption peak due to air-conditioning. Nevertheless, their use is limited, compared to mechanical refrigeration systems, as they are generally larger in size and that limits to a great extend their use in low and medium power applications. For instance a typical value for the volume to refrigeration power ratio in single effect absorption chillers is in the order of 0.04 m^3/kW (without considering the volume occupied by the cooling system) for refrigeration capacities between 10 to 30 kW, whereas mechanical compressor systems can have a ratio equal to 0.02 m^3/kW for the same range of refrigeration capacities. This is a clear inconvenient for the generalization of the absorption technology use limiting its benefits in the contribution to the reduction in CO_2 emissions, particularly for the H_2O-LiBr solution which can work with low heat temperature sources as provided by solar panels.

The absorber is one of the most performance limiting and volume demanding components of absorption systems. In the absorber the concentrated liquid solution absorbs the refrigerant vapor that comes from the evaporator. The main challenge in designing and operating these devices is to maximize the mass transfer rate by getting as much interfacial area as possible. Several configurations for the liquid and vapor streams in the absorber have been proposed in order to increase the heat and mass transfer in the liquid solution: falling films, bubbles, sprays and droplets, liquid jets and sheets, etc... All of them nevertheless present relatively low heat and mass transfer coefficients and lead to large, heavy and rigid heat exchangers. In order to avoid this large volume concern, attempts have been made to scale down the size using, for example, compact heat exchangers, as Plate Heat Exchangers. At present a promising new technology is under study, consisting in the use of membrane contactors in microchannel heat exchangers.

Membrane based absorbers use a microporous polymeric membrane at the solution-refrigerant vapor interface. In the membrane many small diameter pores avoid mixing between vapor and solution, while allow the gas and solution to be in contact. Surface tension prevents the solution from entering the holes,

*Corresponding Author: mdevega@ing.uc3m.es

while the gas diffuses to the solution surface through the pores. In the absorber, the gaseous fluid (typically ammonia or water) passes the membrane and is absorbed by the solution (NH_3-H_2O or H_2O-LiBr respectively) flowing inside constrained flow passages. The vapor pressure difference across the membrane is the driving force for vapor transfer. If the partial pressure of the vapor inside the solution is less than the vapor pressure, it is absorbed at the interface between solution and vapor. Compared with conventional absorption devices there are several advantages of using microporous fiber modules for vapor absorption. These include larger interfacial area per unit volume, independent control of vapor and liquid flow rates, easier scale up, modular design and compactness.

Concerning ammonia-water systems, Chen et al. (2006) theoretically modeled and simulated an absorber using hollow fiber membranes and compared the results to a plate heat exchanger falling film type absorber. In their model, they considered the ammonia–water concentration across this microporous membrane as the driving potential of the refrigerant. The comparisons of fluid phase heat and mass transfer coefficients of both devices revealed that the vast interfacial area feature of the membrane solution is the major reason for achieving higher absorption performance. Schaal et al. (2008) experimentally investigated a NH_3-H_2O absorber using a hollow fiber hydrophobic microporous membrane in order to get basic design data. Ghiasi et al. (2009) conducted experimental research to investigate the absorption of ammonia vapor into the solution with the main objective of the absorber optimization within the whole refrigeration system and the optimization of the system performance.

In H_2O-LiBr applications, Isfahani and Moghaddam (2013) tested an absorber using a superhydrophobic nanofibrous membrane with nominal pore size of 1 micron and 80% porous. They obtained an absorption rate of about 0.006 kg/m^{2}s, using channels of 100 micron thickness and a flow velocity of 5 mm/s. Isfahani et al. (2013) presented a study on the efficacy of highly porous nanofibrous membranes for application in membrane-based absorbers and desorbers. Permeability studies showed that membranes with a pore size greater than about 1 micron are valid for application in the absorber. Ali and Schwerdt (2009) investigated experimentally and analytically the characteristics and properties of commercially available microporous hydrophobic membranes, their influence on the water vapor (refrigerant) mass transfer flux into thin films of aqueous lithium bromide–water solution as well as the limits for utilization in compact absorber design for absorption chillers. Yu et al. (2012) numerically investigated the performance of a membrane-based absorber using the H_2O-LiBr solution. They showed that several folds enhancement in the absorption rate can be achieved respect to conventional absorbers. When the film thickness was reduced from 150 to 50 microns, the absorption rate increased 3-fold. When the solution velocity was quadrupled, the average absorption rate increased 50%. Bigham et al. (2014) showed that mass transport in the microfilm solution could be improved by the implementation of micro-scale features on the flow channel surface. Recently a review of membrane contactors applied in absorption refrigeration systems has been reported by Asfand and Bourouis (2015).

According to the literature review, in order to optimize the process and maximize the vapor absorption rate, detailed studies about the role of the relevant parameters in the absorption process are still necessary. In the present investigation, the water-lithium bromide solution has been selected. This working pair is adequate for evaporation temperatures higher than 0ºC (air conditioning processes) and is the widest used solution worldwide. Moreover, these systems can be fed with low temperature heat. The present study focuses therefore in the absorber modeling of the heat and mass transfer in the micropourous membrane coupled with the cooling of the solution in a H_2O-LiBr absorber.

2. HEAT AND MASS TRANSFER MODELS

The configuration considered for the absorber in the present study is shown in Fig. 1 and Fig. 2. It is a plate-and-frame membrane module with geometrical data and operating variables as described in Table 1. It consists of a vapor channel, the contact membrane, the solution and cooling water channels separated by a stainless steel wall. Water-lithium bromide solution is used.

Table 1 Data considered for the simulation, corresponding to the schemes of the absorber represented in Fig. 1 and 2.

Parameter	Value
Active layer material	PTFE
Cooling water inlet temperature, T_{cw} (ºC)	25
Solution inlet temperature, T_s (ºC)	25
Vapor inlet temperature, T_v (ºC)	12
Membrane pore diameter, d_p (m)	10^{-6}
Vapor pressure, P_v (kPa)	1.37
Porosity, ε	0.8
Cooling water channel height, e_{cw} (m)	$0.2 \cdot 10^{-3}$
Stainless steel wall thickness, e_w (m)	$0.5 \cdot 10^{-3}$
Solution channel height, e_s (m)	$0.2 \cdot 10^{-3}$
Membrane thickness, e_m (m)	$60 \cdot 10^{-6}$
Vapor channel height, e_v (m)	0.02
Cooling water channel width, l_{cw} (m)	$2.5 \cdot 10^{-3}$
Solution channel width, l_s (m)	10^{-3}
Vapor channel width, l_v (m)	0.3
Number of solution channels	200
Number of cooling water channels	100
Length of channels (m)	0.2
Discretization length (m)	$2 \cdot 10^{-3}$
Total solution mass flow rate at the inlet (kg/s)	$5 \cdot 10^{-3}$
Total cooling water mass flow rate (kg/s)	$5 \cdot 10^{-3}$
Vapor mass flow rate at the inlet (kg/s)	$5 \cdot 10^{-4}$
LiBr mass fraction at the inlet, x	0.6

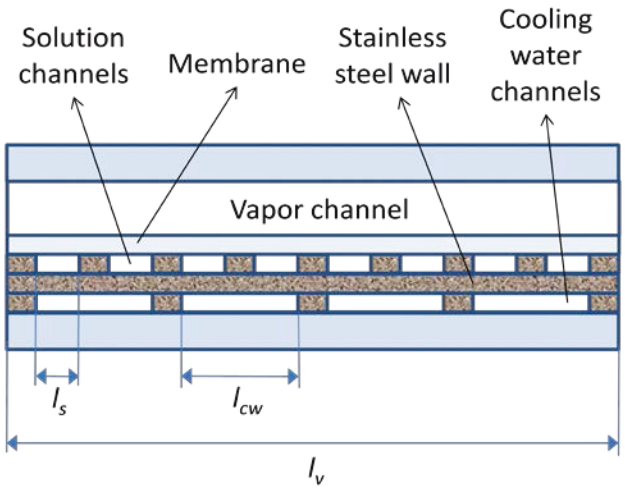

Fig. 1 General scheme of the absorber.

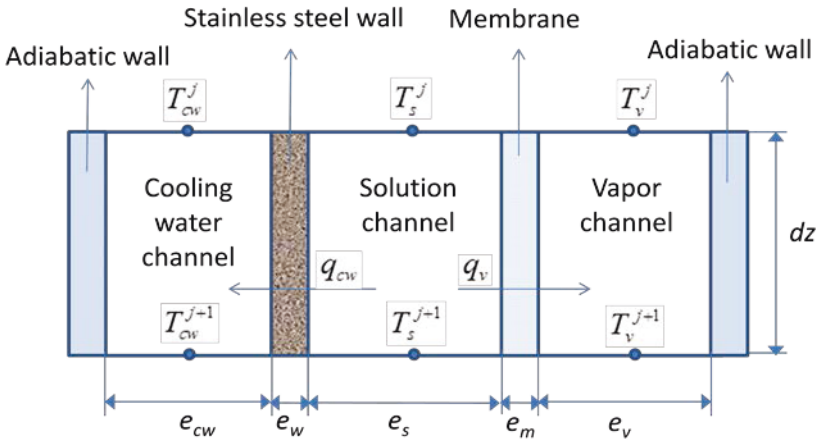

Fig. 2 Differential element of the absorber.

2.1 Type of Flow across the Membrane

To calculate the mass flux through the membrane, the flow regime must first be determined. Knudsen number *Kn* is used to evaluate the transport of water vapor across the membrane: when $Kn < 0.01$, collisions between gas molecules dominate and viscous flow occurs, resulting in rapid convective transport. When $Kn \geq 10$ collisions between molecules and pore wall are dominant and the gas transport takes place via Knudsen flow (free molecular regime). Transitional regime exists if $0.1 < Kn < 10$. Knudsen number is defined as:

$$Kn = \frac{\lambda}{d_p} \tag{1}$$

where λ is the mean free path of the water vapor (distance between molecular collisions) and d_p is the membrane pore diameter. In this work, the mean free path is calculated using the equation given by Zhang (2008):

$$\lambda = \frac{c_B T}{\sqrt{2}\pi\sigma^2 P_m} \tag{2}$$

where c_B is the Boltzmann constant ($1.38 \cdot 10^{-23}$ J/K), T is the absolute temperature (K), σ is the molecular collision diameter (2.641 Å for water vapor) and P_m is the mean total pressure within the membrane pores (Pa).

For the current study, the calculated Knudsen number value is in the range between $9.48 < Kn < 9.98$ and consequently, a transition between Knudsen and Poiseuille flows is present.

2.2 Mass Transfer Model

Mass flow rate of vapor transported across the membrane and absorbed by the solution is calculated in the present work referring the conditions to the bulk water vapor and bulk aqueous solution streams:

$$\dot{m}_{va}^{j} = J^{j} \cdot A \tag{3}$$

where A is the heat and mass transfer area:

$$A = l_s \cdot dz \tag{4}$$

and J is the absorption rate:

$$J^j = \frac{P_v - P_s^j}{R_{ov}^j} \tag{5}$$

P_v and P_s are the bulk vapor pressure and the water vapor partial pressure corresponding to the bulk solution concentration (x) and temperature (T_s). The overall mass transfer resistance between the bulk water vapor and bulk aqueous solution (R_{ov}) includes the resistance to diffusion through the aqueous solution boundary layer (R_s) and resistance to diffusion of water vapor through the membrane active layer (R_m). Both resistances act in series:

$$R_{ov}^j = R_s^j + R_m^j \tag{6}$$

Taking into account the case analyzed in this work, where a transition between Knudsen and Poiseuille flows is present in the membrane pores, a parallel system is obtained for the resistances to mass transfer inside the membrane (Fig. 3):

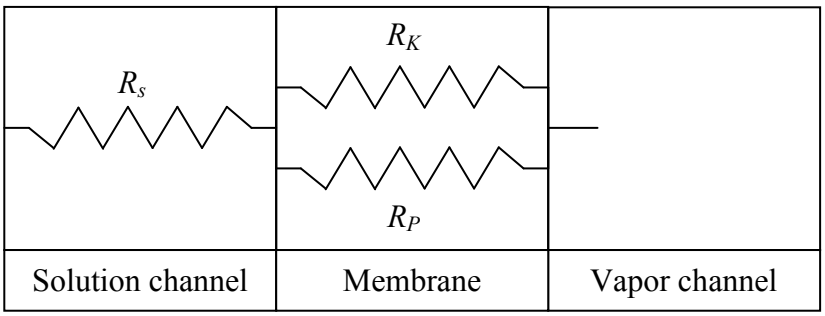

Fig. 3 Mass transfer resistances in the absorber.

The equivalent mass resistance of the membrane can be obtained as

$$\frac{1}{R_m^j} = \frac{1}{R_K^j} + \frac{1}{R_P^j} \tag{7}$$

where the first term, in Eq. (7) is the contribution of Knudsen flow to the mass transfer and the second one that of the Poiseuille flow.

In Eq. (7), all resistances can be calculated as in Eq. (8), because parallel channels of rectangular cross-section are considered, being K the mass transfer coefficient:

$$\frac{1}{R^j} = K^j \tag{8}$$

According to the Dusty-Gas model, described in Mason and Malinauskas (1983) and applied by Yu et al. (2012) to a similar problem, the mass transfer coefficient through the membrane K_m, can be estimated as:

$$K_m = -\frac{M}{e_m}\left(\frac{D_e^K}{RT} + \frac{P_m B_0}{RT\mu_v}\right) \tag{9}$$

Where the diffusion term can be evaluated as:

$$D_e^K = K_0 \left(\frac{8RT}{\pi M} \right)^{0.5} \tag{10}$$

$$K_0 = \frac{\varepsilon d_p}{3\tau} \tag{11}$$

And the molar viscous flow contribution can be calculated from:

$$B_0 = \frac{\varepsilon d_p^2}{32\tau} \tag{12}$$

In Eq. (9), M is the molecular weight of water, e_m is the membrane thickness, R is the universal gases constant and μ_v refers to the vapor viscosity. In Eq. (11) and (12), ε and τ are the porosity and tortuosity of the membrane, respectively. Tortuosity of the membrane is calculated as a function of the membrane porosity, according to Iversen et al. (1997):

$$\tau = \frac{(2-\varepsilon)^2}{\varepsilon} \tag{13}$$

Resistance to mass transfer inside the bulk solution R_s can be calculated according to Ali and Schwerdt (2009), as:

$$R_s^j = \frac{P_{sat}^j}{\rho_w^j k_s^j} \tag{14}$$

where P_{sat} is the saturated water pressure corresponding to the bulk solution temperature, ρ_w is the liquid water density and k_s is the mass transfer coefficient between the solution-vapor interface and the bulk aqueous solution. This last parameter is calculated using the correlation derived by Schuster et al. (2008):

$$Sh = 0.78\, Re_{rel}^2 + 0.43\, Re_{rel} + 5.07 \tag{15}$$

where:

$$Sh = \frac{k_s D_h}{D} \tag{16}$$

$$Re_{rel} = \frac{D_h \rho u_{rel}}{\mu} \tag{17}$$

and:

$$u_{rel} = u_{v,i} - u_{s,i} \tag{18}$$

$u_{s,i}$ is the solution velocity at the interface and $u_{v,i}$ is the vapor velocity at the same position. In this study the last velocity is considered to be negligible.

In Eqs. (16) and (17), D_h is the hydraulic diameter, ρ, u and μ are the density, velocity and viscosity of the solution, respectively, and D refers to the diffusion coefficient of water in the solution. In this study, the diffusion coefficient was corrected by temperature using the equation described by Mittermaier et al. (2014):

$$D = D(25\ ^{\circ}\mathrm{C})\frac{T+273.15}{298.15}\frac{\mu(25\ ^{\circ}\mathrm{C})}{\mu(T)} \tag{19}$$

where diffusion coefficient at 25 ºC is calculated as:

$$D(25\ ^{\circ}\mathrm{C}) = \left(1.3528 + 0.19881b - 0.036382b^2 + 0.0020299b^3 - 0.000039375b^4\right)10^{-9} \tag{20}$$

Parameter b in Eq. (20) is the molality, obtained from:

$$b = \frac{x}{M_{LiBr}(1-x)} \tag{21}$$

M_{LiBr} is the molecular weight of the lithium bromide.

2.3 Heat Transfer Model

Energy rate balance applied to the differential element j is written as:

$$\left(\dot{m}_{va} i_{lv}\right)^j = q_s^j + q_v^j + q_{cw}^j \tag{22}$$

Left term in Eq. (22) corresponds to the thermal power released during absorption of the vapor flow rate $\dot{m}_{va}$ into the solution. Right terms are related to the heat transferred to the solution, vapor and cooling water respectively. These can be calculated as:

$$q_s^j = \left(\dot{m}i\right)_s^{j+1} - \left(\dot{m}i\right)_s^j \tag{23}$$

$$q_{cw}^j = \dot{m}_{cw}\left(i_{cw}^{j+1} - i_{cw}^j\right) = \dot{m}_{cw} Cp_{cw}^j \left(T_{cw}^{j+1} - T_{cw}^j\right) \tag{24}$$

$$q_v^j = \dot{m}_v^j Cp_v^j \left(T_v^{j+1} - T_v^j\right) \tag{25}$$

Mass rate balances for solution and vapor give the mass flow rates in the differential element j+1*:*

$$\dot{m}_s^{j+1} = \dot{m}_s^j + \dot{m}_{va}^j \tag{26}$$

$$\dot{m}_v^{j+1} = \dot{m}_v^j - \dot{m}_{va}^j \tag{27}$$

Mass fraction of lithium bromide in the solution is calculated from:

$$x^{j+1} = x^j \frac{\dot{m}_s^j}{\dot{m}_s^{j+1}} \tag{28}$$

Last term of Eq. (24) considers that cooling water is an incompressible liquid with constant specific heat and neglects the pressure drop along the channel. Similarly, right hand term in Eq. (25) considers that vapor is an ideal gas with constant specific heats.

The present model also considers that heat is transferred from the bulk solution channel (where absorption takes place) to both cooling water and vapor channels. In this case the following relations are also valid:

$$q_{cw}^{j} = U_{s-cw}^{j} A\left(T_{s}^{j} - T_{cw}^{j}\right) \tag{29}$$

$$q_{v}^{j} = U_{s-v}^{j} A\left(T_{s}^{j} - T_{v}^{j}\right) \tag{30}$$

The global heat transfer coefficients in Eqs. (29) and (30) are calculated as:

$$\frac{1}{U_{s-cw}^{j}} = \frac{1}{h_{cw}^{j}} + \frac{e_{w}}{k_{w}^{j}} + \frac{1}{h_{s}^{j}} \tag{31}$$

$$\frac{1}{U_{s-v}^{j}} = \frac{1}{h_{v}^{j}} + \frac{e_{m}}{k_{m\,a}^{j}} + \frac{1}{h_{s}^{j}} \tag{32}$$

In Eq. (31), the convection heat transfer coefficient for cooling water has been calculated using correlation developed by Koyuncuoglu et al. (2012) for microchannels:

$$Nu = 0.032\, Re^{0.804}\, Pr^{0.03} \tag{33}$$

where:

$$Re = \frac{D_h \rho u}{\mu} \tag{34}$$

$$Pr = \frac{\mu}{c_p k} \tag{35}$$

In Eqs. (31) and (32), the convection heat transfer coefficients for the solution and vapor have been calculated using mass and heat transfer analogy, based on correlation obtained by Gabelman and Hwang (1999) for a rectangular module:

$$Nu = 0.18\, Re^{0.86}\, Pr^{0.33} \tag{36}$$

The average thermal conductivity of the membrane $k_{m,a}$ is calculated using the equation given by Martínez and Rodríguez-Maroto (2006):

$$k_{m,a} = \varepsilon k_{v} + \left(1 - \varepsilon\right) k_{m} \tag{37}$$

In Eq. (37), k_v is the thermal conductivity of the vapor inside the membrane pores, while k_m is the thermal conductivity of the membrane solid material, in this case equal to 0.22 W/mK.

The heat and mass transfer models described in previous sections have been implemented in Engineering Equation Solver software, EES™ (Klein, 2014). Thermodynamic properties of water-lithium bromide

solution have been calculated using EES, which uses correlations developed by Patek and Klomfar (2006) for all properties, except for viscosity and thermal conductivity. In this case EES uses correlations provided by DiGuilio et al. (1990). Thermodynamic properties of water also are calculated using EES and the correlation of Harr et al. (1984) and transport properties using correlations from Electrical Research Association (1967). Thermal conductivity of stainless steel AISI347 is calculated using data of Ho and Chu (1977).

3. RESULTS AND DISCUSSION

Results are shown for calculated variables at different distances from the channel entrance, using co-fluxes configuration.

In Fig. 4 the variation of the absorption rate along the channel is represented simultaneously with the solution concentration change. The decrease in LiBr mass fraction describes the water vapor absorption process. The decrease is similar to the one found in Yu et al. (2012). At the channel entrance when the higher pressure potential is available (Fig. 5) the absorption rate is higher. This value tends to decrease as the solution absorbs the vapor along the channel, and the driving potential (the difference in pressure) decreases. This is confirmed by the evolution of the pressure potential shown in Fig. 5, which decays almost exponentially.

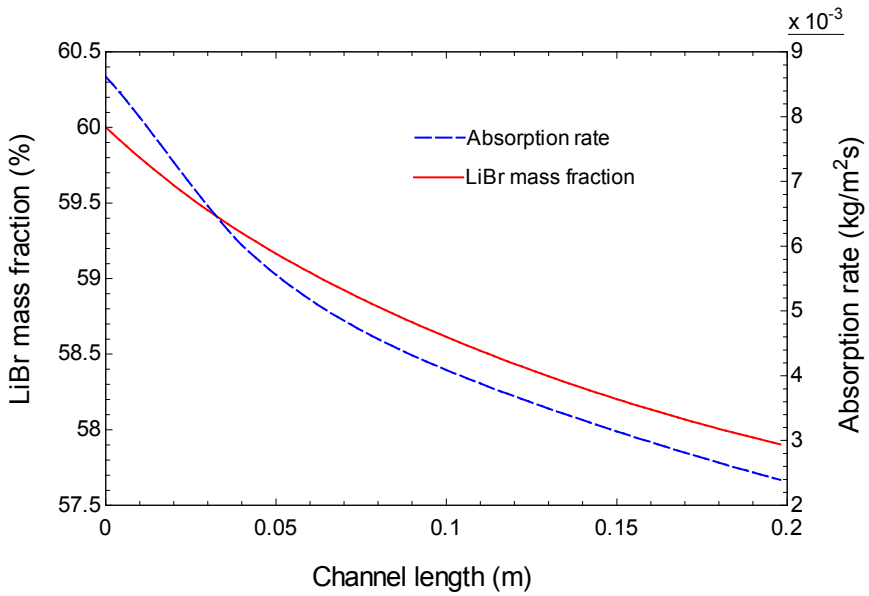

Fig. 4 Evolution of the LiBr mass fraction and absorption rate along the absorption channel.

Fig. 5 also shows the overall mass transfer coefficient obtained. Values obtained are of the same order of magnitude of those reported by Isfahani and Moghaddam (2013).

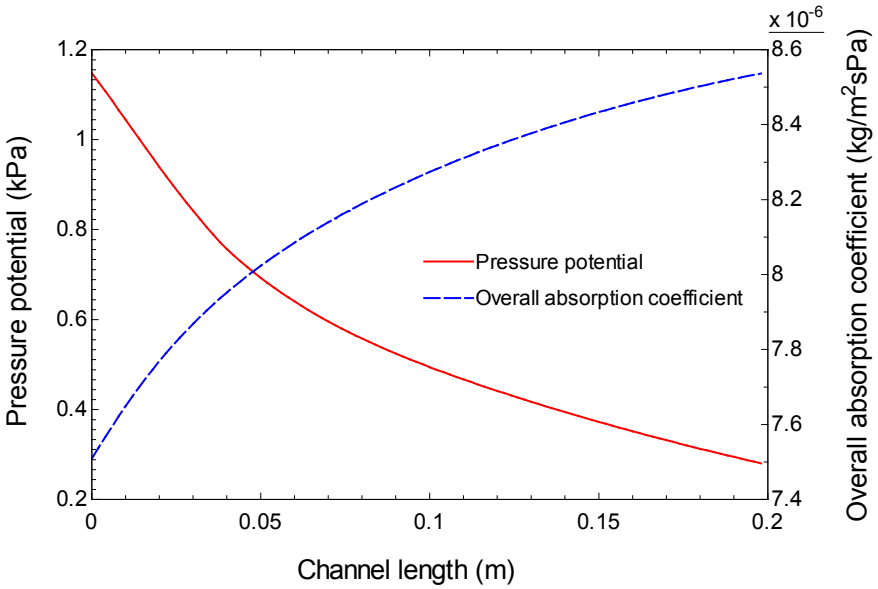

Fig. 5 Evolution of the pressure potential and overall absorption coefficient along the absorption channel.

Variation of the solution and cooling water temperature along the absorption channel is shown in Fig. 6. The release of the heat of absorption is high near the entrance of the channel and at first the temperature of the solution increases quickly. Nevertheless, beyond approximately 5 cm in the channel, as the absorption rate decays and the heat is diffused to the cooling water channel, the bulk temperature of the solution increases slowly. If the cooling water flow rate is reduced, temperature trends similar to those found by Bigham et al. (2014) are obtained.

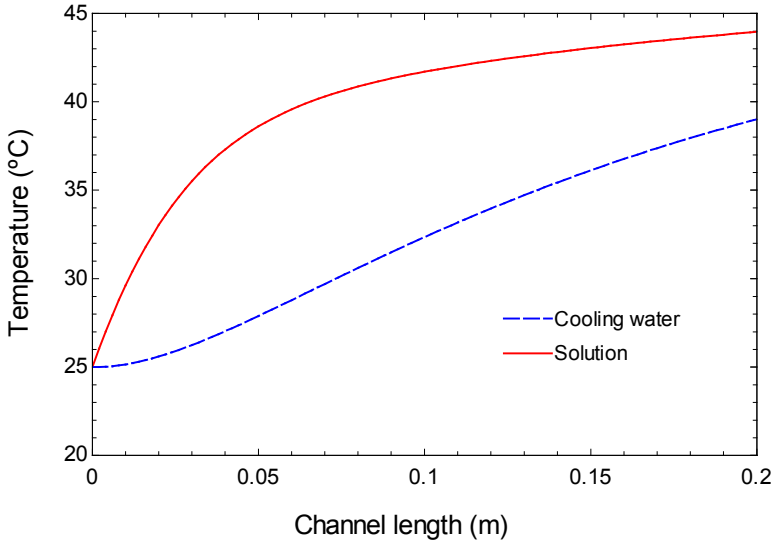

Fig. 6 Evolution of the solution and cooling water temperature along the absorption channel.

According to Fig. 7, where the evolution of the thermal power transferred to the cooling water and vapor and stored in the solution along the absorption channel is represented, in the first 3 cm of the channel, most of the power is stored in the solution. After 5 cm length (corresponding to the solution temperature variation commented in relation to Fig. 6), heat is most effectively transferred to the cooling water. The contribution of the power transferred to the vapor is two orders of magnitude smaller.

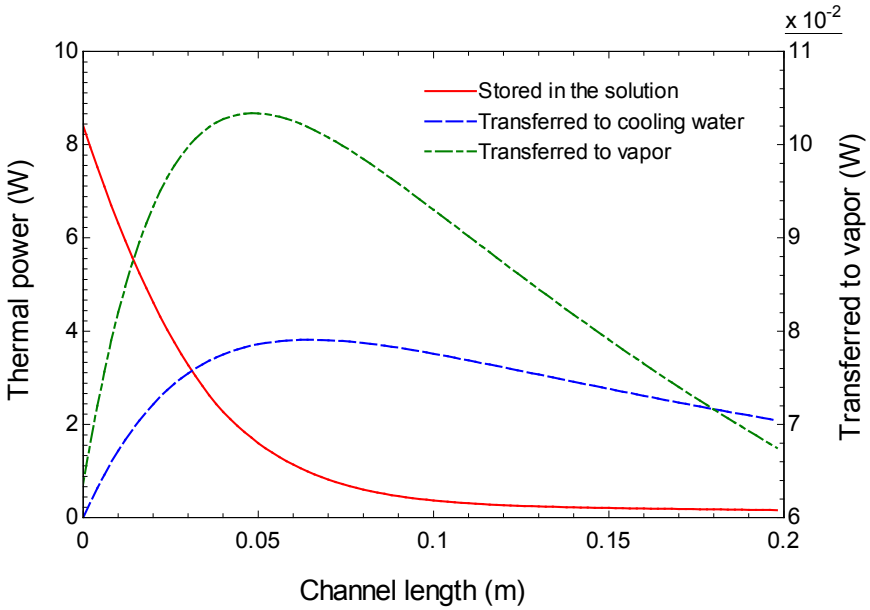

Fig. 7 Evolution of the thermal power transferred to the cooling water and vapor and stored in the solution along the absorption channel.

An experimental test rig is being constructed at present in Universidad Carlos III de Madrid (UC3M), Spain, in order to validate the simulated results and evaluate the capabilities of different types of micro heat exchangers configurations, membranes and operating conditions.

5. CONCLUSIONS

In the present paper a simulation of the heat and mass transfer processes taking place in a miniaturized absorber using membrane technology has been developed. The following conclusions have been derived:

- High mass transfer rates are obtained using the configuration analyzed, higher than some studies reported in the open literature using conventional falling film absorbers.
- The first 5 cm of the absorption channels are the most active for mass transfer.
- Correlations used in the model to predict heat and mass transfer coefficients have a high influence on the results obtained. An experimental validation is required.
- Mass fraction changes of about 2% are obtained for the conditions simulated in the present study using an absorber of 20 cm length.
- The absorber simulated has dimensions of 0.3 x 0.2 x 0.022 m^3, corresponding to an absorption chiller of 448 W cooling capacity. Dimensions can be considerably reduced optimizing the design.

ACKNOWLEDGMENT

The financial support of this study by the Ministerio de Economía y Competitividad of Spain through the research grant ENE2013-43131-R is greatly appreciated.

REFERENCES

[1] Chen, J., Chang, H., Chen, S.-R., "Simulation study of a hybrid absorber-heat exchanger using hollow fiber membrane module for the ammonia-water absorption cycle," *Int. J. Refrig.*, 29, pp. 1043-1052, (2006).

[2] Schaal, F., Weimer, T., Hasse, H., "Membrane Contactors for Absorption Refrigeration," *International Sorption Heat Pump Conference*, Seoul, Korea, (2008).

[3] Ghiasi, C., Martí-Calatayud, M.C., Weimer, T., Ziegler, F., "Ammonia-water absorption heat pumps with membrane absorber," *IIR Conference: Ammonia Refrigeration Technology*, Ohrid, (2009).

[4] Isfahani, R.N. and Moghaddam, S., "Absorption characteristics of lithium bromide (LiBr) solution constrained by superhydrophobic nanofibrous structures," *Int. J. Heat Mass Transf.*, 63, pp. 82-90, (2013).
[5] Isfahani, R.N., Sampath, K., and Moghaddam, S., "Nanofibrous membrane-based absorption refrigeration system," *Int. J. Refrig.*, 36, pp. 2297-2307, (2013).
[6] Ali, A.H.H. and Schwerdt, P., "Characteristics of the membrane utilized in a compact absorber for lithium bromide-water absorption chillers," *Int. J. Refrig.*, 32, pp. 1886-1896, (2009).
[7] Yu, D., Chung, J., Moghaddam, S., "Parametric study of water vapor absorption into a constrained thin film of lithium bromide solution," *Int. J. Heat Mass Transf.*, 55, pp. 5687-5695, (2012).
[8] Bigham, S., Yu, D., Chugh, D., Moghaddam, S., "Moving beyond the limits of mass transport in liquid absorbent microfilms through the implementation of surface-induced vortices," *Energy,* 65, pp. 621-630, (2014).
[9] Asfand, F. and Bourouis, M., "A review of membrane contactors applied in absorption refrigeration systems," *Renew. Sust. Energ. Rev.,* 45, pp. 173-191, (2015).
[10] Zhang, L.-Z., "A fractal model for gas permeation through porous membranes," *Int. J. Heat Mass Transf.*, 51, pp. 5288–5295, (2008).
[11] Mason, E.A. and Malinauskas, A.P., *Gas Transport in Porous Media: The Dusty-Gas Model*, Elsevier, (1983).
[12] Iversen, S.B., Bhatia, V.K., Dam-Johansen, K., Jonsson, G., "Characterization of microporous membranes for use in membrane contactors," *J. Membr. Sci.*, 130, pp. 205-217, (1997).
[13] Schuster, A., Sefiane, K., Ponton, J., "Multiphase mass transport in mini/micro-channels microreactor," *Chem. Eng. Res. Des.*, 86, pp. 527-534, (2008).
[14] Mittermaier, M., Schulze, P., Ziegler, F., "A numerical model for combined heat and mass transfer in a laminar liquid falling film with simplified hydrodynamics," *Int. J. Heat Mass Transf.* 70, pp. 990-1002, (2014).
[15] Koyuncuoglu, A., Jafari, R., Okutucu-Özyurt, T., Külah, H., "Heat transfer and pressure drop experiments on CMOS compatible microchannel heat sinks for monolithic chip cooling applications," *Int. J. Therm. Sci.*, 56, pp. 77-85, (2012).
[16] Gabelman, A., Hwang, S.T., "Hollow fiber membrane contactors," *J. Membr. Sci.*, 159, pp. 61-106, (1999).
[17] Martínez, L., Rodríguez-Maroto, J.M., "Characterization of membrane distillation modules and analysis of mass flux enhancement by channel spacers," *J. Membr. Sci.*, 274, pp. 123-137, (2006).
[18] Klein, S.A., *Engineering Equation Solver*. Academic Professional, 1992-2014, V9.698-3D, 2014.
[19] Patek, J. and Klomfar, J., "A computationally effective formulation of the thermodynamic properties of LiBr-H2O from 273 to 500 K over full composition range," *Int. J. Refrig.*, 29, pp. 566-578, (2006).
[20] DiGuilio, R.M., Lee, R.J., Jeter, S.M., Teja, A.S., "Properties of Lithium Bromide-Water Solutions at High Temperatures and Concentrations - I Thermal Conductivity," *ASHRAE Trans.*, Paper 3380, RP-527, pp. 702-708, (1990).
[21] Harr, L., Gallagher, J.S., Kell, G.S., "*NBS/NRC Steam Tables*", Hemisphere Publishing Co., (1984).
[22] Electrical Research Association, "*Steam Tables, Thermodynamic Properties of Water and Steam; Viscosity of Water and Steam, Thermal Conductivity of Water and Steam*", Edward Arnold Publishers, London, (1967).
[23] Ho, C.Y. and T.K.Chu, "Electrical Resistivity and Thermal Conductivity of Nine Selected AISI Stainless Steels," *CINDAS Report 45*, Sep. (1977).